AGU ADVANCING EARTH AND SPACE SCIENCES

JGR Space Physics

RESEARCH ARTICLE
10.1029/2024JA033492

Key Points:

- Investigation of the SuperMAG SMR local time index during geomagnetic disturbances identified by a new SOPHIE-M substorm list
- Dawn geomagnetic disturbances occur during dawn-dusk asymmetry in the low latitude current system suggesting a dawnside current wedge
- Multiple intensification periods identified in SOPHIE-M are linked to asymmetries in the dawn-dusk SMR index

Correspondence to:
G. E. Bower,
geb23@leicester.ac.uk

Citation:
Bower, G. E., Milan, S. E., Imber, S., Schillings, A., Fleetham, A., Beggan, C., & Gjerloev, J. W. (2025). Asymmetry in the ring current during geomagnetic disturbances. *Journal of Geophysical Research: Space Physics*, *130*, e2024JA033492. https://doi.org/10.1029/2024JA033492

Received 31 OCT 2024
Accepted 12 FEB 2025

Asymmetry in the Ring Current During Geomagnetic Disturbances

G. E. Bower[1], S. E. Milan[1], S. Imber[1], A. Schillings[1,2], A. Fleetham[1], C. Beggan[3], and J. W. Gjerloev[4]

[1]School of Physics and Astronomy, University of Leicester, Leicester, UK, [2]Department of Physics, Umeå University, Umeå, Sweden, [3]British Geological Survey, Edinburgh, UK, [4]Johns Hopkins University Applied Physics Laboratory, Laurel, MD, USA

Abstract Geomagnetic disturbances (GMDs) are defined as rapid changes in the magnetic field of the Earth that can lead to geomagnetically induced currents (GICs). Recent studies have shown that there are two main populations of GMDs, one in the pre-midnight sector and one in the dawn sector. The pre-midnight GMDs have been related to the substorm current wedge. The dawn population of GMDs has previously been found to occur during multiple intensification events. We adapt the SOPHIE substorm list to identify more instances of multiple intensifications. Recent models suggest the formation of a "dawnside current wedge" (DCW) during the main phase of storms that could lead to dawn sector GMDs. We investigate GMDs at all latitudes using the SuperMAG local time indices (SMR-LT), where SMR-LT are local time measurements of the magnetic field at low latitudes. During multiple intensification events the dawn sector low latitude magnetic field between 3 and 9 MLT (SMR06) is typically higher than the dusk sector between 15 and 21 MLT (SMR18), which is indicative of a DCW. Statistical analysis of the local time ring current indices during the dawn and pre-midnight GMDs shows that the dawn GMDs occur when the difference between the dawn sector and dusk sector SMR values (SMR06-SMR18) is largest and thus when there is a DCW.

Plain Language Summary Rapid changes in the magnetic field of the Earth can lead to electrical currents that flow at the Earth's surface and can cause problems for grounded infrastructure such as pipelines and high voltage power grids. These rapid changes are called geomagnetic disturbances (GMDs), and have been previously shown to predominately occur within the dawn and pre-midnight locations. The pre-midnight GMDs have been related to a nightside phenomenon called substorms. The morning population has been shown to occur during periods of strong periodic variations of the magnetic field called multiple intensifications. We adapt an existing list of substorms occurrence to identify periods of multiple intensifications. Recent research has suggested that during a geomagnetic storm, where the magnetic field is compressed, current flows form at dawn, called the "dawnside current wedge" (DCW), that could lead to GMDs. We investigate the local time measurements of the magnetic field at low latitudes using the SuperMAG SMR-LT indices, which is a measure of the Earth's ring current. Statistical analysis of the SMR-LT values during the dawn and pre-midnight GMDs supports the hypothesis of a dawn current wedge. This finding suggests that dawn and pre-midnight GMDs form through different processes but can occur at the same time.

1. Introduction

Space weather events can cause large and rapid variations in the magnetic field of the Earth which can drive currents that flow though the surface of the Earth called geomagnetically induced currents (GICs). GICs can cause problems when they flow through grounded infrastructure such as power lines and the rail network (Albertson et al., 1973; Campbell, 1978; Marshall et al., 2010; Patterson et al., 2024). The causes of GICs are often investigated via the rapid fluctuations in the magnetic field measured from the ground ($d\mathbf{B}/dt$) which are caused by electrical currents flowing in the ionosphere (Pulkkinen et al., 2008; Rogers et al., 2021; Viljanen, 1997). The large $d\mathbf{B}/dt$ are called "spikes" or geomagnetic disturbances (GMDs) (Milan et al., 2023; Schillings et al., 2022). These ionospheric currents are part of larger current systems that flow in the ionosphere and magnetosphere. This study investigates the ring current during the GMDs using the SuperMAG SMR local time indices (SMR-LT) which are measures of the partial ring current separated by magnetic local time (MLT) (Newell & Gjerloev, 2012).

GMDs have previously been shown to occur in geomagnetic ground observatory measurements at two main hot-spots, pre-midnight and dawn. The pre-midnight population has been suggested to be associated with substorm activity due to the formation of the substorm current wedge and the associated substorm electrojet (Fleetham et al., 2024; Juusola et al., 2015; Schillings et al., 2022; Weigel et al., 2002).

The dawn GMDs have been suggested to be due to omega bands which are an auroral wave-like feature, in the shape of an omega, that drift eastward and can occur in the morning sector (Apatenkov et al., 2020; Juusola et al., 2015; Partamies et al., 2017; Schillings et al., 2022). However, this has been disputed by Zou et al. (2022) who found GMDs occur for many auroral drivers such as poleward expanding auroral bulges, auroral streamers, poleward boundary intensifications, omega bands and pulsating auroras. Ngwira et al. (2018) has also suggested Pc5 waves as a possible cause. A simulation by Sorathia et al. (2023) suggests that auroral streamers are a counterpart of bursty bulk flows (BBFs) on the dawnside of the magnetosphere which produce rapidly varying magnetic perturbations on the ground. More recently Milan et al. (2024) showed that the dawn spikes occur during "multiple intensification" convection states. This is described by Milan et al. (2021) as prolonged rapid quasi-periodic variations in the auroral activity index, AL, associated with an expanded auroral oval. Milan et al. (2024) also showed that dawn spikes are not directly related to substorms but are related to streamer-like auroral activity occurring within the westward electrojet. The results from Sorathia et al. (2023) are similar to the multiple intensification events described by Milan et al. (2021). Sorathia et al. (2023) also related BBFs to a "dawnside current wedge" (DCW) that is distinct from the substorm current wedge and forms due to a dawn-dusk asymmetry in the ring current during storm times.

Sorathia et al. (2023) built on the work of Ohtani (2021) who first investigated four GIC events using the SuperMAG SMR local time indices to study the partial ring current during the events. The events took place during storms with an enhanced westward electrojet which was initially observed postmidnight and then extended eastward covering the entire dawn sector. Ohtani et al. (2018) suggested this was related to a "dawnside current wedge" (DCW) that is closed via downward and upward field aligned currents at its eastern and western ends respectively. They suggest that the formation of the DCW and expansion toward dayside is an ionospheric projection of the magnetotail current reduction extending toward the dawnside flank. In Ohtani (2021) they investigated the SuperMAG geomagnetic indices during the main phase of 693 storms between 1996 and 2018. They showed that the dawn-dusk asymmetry of the storm-time ground magnetic depression is correlated with the enhancement of the dawnside westward auroral electrojet and suggested this is associated with the DCW driven by a substorm-like process. Recently Ohtani et al. (2023) have investigated four scenarios that can cause an intensification of the dawnside electrojet. They show an event which fits each of their scenarios but suggest that substorm injection of energetic electrons is the cause of the majority of the events.

The motivation for this study is to statistically investigate the partial ring current, using SuperMAG SMR local time (LT) indices, during geomagnetic disturbances that could lead to ground induced currents particularly during multiple intensification convection state. This will allow us to understand how GMDs during multiple intensification convection state differs from GMDs that occur during typical substorm expansion phases. Section 2 describes a newly adapted SOPHIE substorm list to identify multiple intensification convection state as described by Milan et al. (2021). SOPHIE (Substorm Onsets and Phases from Indices of the Electrojet) is a well established substorm list from Forsyth et al. (2015) used in many studies (Clilverd et al., 2021; Coxon et al., 2023; Freeman et al., 2019). SOPHIE provides continuous classifications of each minute for which substorm phase it occurs in based on the SuperMAG AL and AU indices. Further description is provided in Section 2. The SuperMAG SMR data is also described in Section 2. Three example events are shown in Section 3 along with a statistical study on the SMR local time (SMR-LT) values at the time of the GMDs. Section 4 discusses the results and Section 5 concludes.

2. Data

Ground based magnetometer data, obtained from the SuperMAG network (Gjerloev, 2012), has been used to identify GMDs. SuperMAG data are provided at 1 s resolution, have a baseline removed, and are rotated into a N, E, Z coordinate system, where N is the North-South geomagnetic direction with positive northward, E is the East-West direction with positive eastward and Z is the vertical direction with positive downwards. We use the GMD list generated by the Bower, Imber, Milan, Schillings, et al. (2024) algorithm which detects GMDs with a minimum of 50 nT change in 10 s in any direction. The distribution of stations used is shown in Bower, Imber, Milan, Schillings, et al. (2024) Figure 4c. We used the data for the years 2010–2021. This gives a list of 136,011 GMD, with 45,208 at dawn between 2 and 9 magnetic local time (MLT), 87,402 at pre-midnight between 17 and 2 MLT and 3401 on the dayside between 9 and 17 MLT.

Milan et al. (2021) analyzed the variation in magnetospheric convection state during the year 2010 using the orientation and magnitude of the interplanetary magnetic field (IMF) and the auroral upper and lower electrojet indices AU and AL from the OMNI data set (King & Papitashvili, 2005). They also used the region 1 and 2 field aligned currents (FACs) from the Active Magnetosphere and Planetary Electrodynamics Response Experiment (AMPERE) and the polar cap size calculated using boundary between the region 1 and region 2 FACs as described by Milan et al. (2015). This is done by finding the zero point crossing between the region 1 and region 2 field aligned currents (FACs) from the AMPERE data maps and fitting a circle to these points. Milan et al. (2021) define eight convection states, quiet, weak, substorm growth phase, substorm expansion phase, substorm driven phase, substorm recovery phase, recovery bay and multiple intensification. For simplicity this classification scheme will be referred to as the Milan list throughout the rest of this study.

The convection state of main interest here is the multiple intensification state. An example of the multiple intensification state is presented in Figure 1a, which shows the variation of AU and AL over a 60 hr period starting on 28 May 2010, which is also discussed in Milan et al. (2024). Two classic isolated substorms are seen around 4 and 9 hr. These are each around 3 hr in duration, with growth, expansion, and recovery phases an hour each in duration. Another clear substorm growth followed by expansion phase is seen between 21 and 24 hr, but this is followed by driven activity. Between 28 and 40 hr this activity takes the form of repeated, short period intensifications of AL, which is clearly different in nature from classic substorm activity. This is the behavior termed "multiple intensifications" by Milan et al. (2021). Milan et al. (2024) went on to show that this activity is produced by intensifications of the westward electrojet in the dawn sector, not the substorm electrojet in the pre-midnight sector. While substorms are associated with an expansion and contraction of the polar cap, the polar cap tends to remain uniform in size during multiple intensifications (Milan et al., 2021).

Milan et al. (2024) shows that the dawn GMDs occur most frequently during this multiple intensification state. Pre-midnight GMDs do occur during the multiple intensification state, but also during the substorm expansion, driven phase and the recovery bay state. In order to further investigate the multiple intensification state, we adapt the SOPHIE (Substorm Onsets and Phases from Indices of the Electrojet) substorm list (Forsyth et al., 2015) to identify multiple intensification states. This allows us to investigate more active years as the Milan list is only available for 2010.

The original SOPHIE substorm list classifies periods of growth phase, expansion phase and recovery phase. It also has a flag denoting enhanced convection. It works by using the SuperMAG SML index and using its rate of change (dSML/dt) to classify expansion and recovery phases. All other times are growth phase. A manually set expansion percentile (EPT) value is used to define expansion phases and a recovery percentile (RPT) is iteratively modified to minimize the difference between the number of expansion and recovery phases. Full details on the SOPHIE list can be found in Forsyth et al. (2015). It is important to note that for small EPT more substorms are identified and expansion phase onset is moved to an earlier time (Forsyth et al., 2015). This study uses the EPT 90 list (Forsyth, 2024), a threshold used by Freeman et al. (2019) to give a conservative estimate of the amount of time spent in the expansion and recovery phase.

Figure 1b shows an example of the substorm phases identified by the SOPHIE algorithm. Blue is the growth phase, lilac is the expansion phase, pink is the recovery phase and red is the enhanced convection. It successfully identifies many of the true substorms occurring during the interval, but also misidentifies many of the multiple intensifications as individual substorms. We also see that anything that is not an expansion or a recovery phase is labeled as a growth phase, including long periods of quiescence.

This 90 EPT SOPHIE list is the basis of a new SOPHIE-M list which differentiates between multiple intensifications and substorms. It does this by using the distinction that substorms are associated with variations in the size of the polar cap, while multiple intensifications are not, hence, we test if the radius of the boundary between the region 1 and region 2 field aligned current (FACs) is constant and not varying. The values for the FAC boundary are calculated by Milan et al. (2015) using the AMPERE data, to find the zero point crossing between the region 1 and region 2 field aligned currents (FACs) and fit a circle to these points. Each fit has an associated goodness of fit metric as an indication of how reliable the fit is. Figure 1d shows the FAC radius in

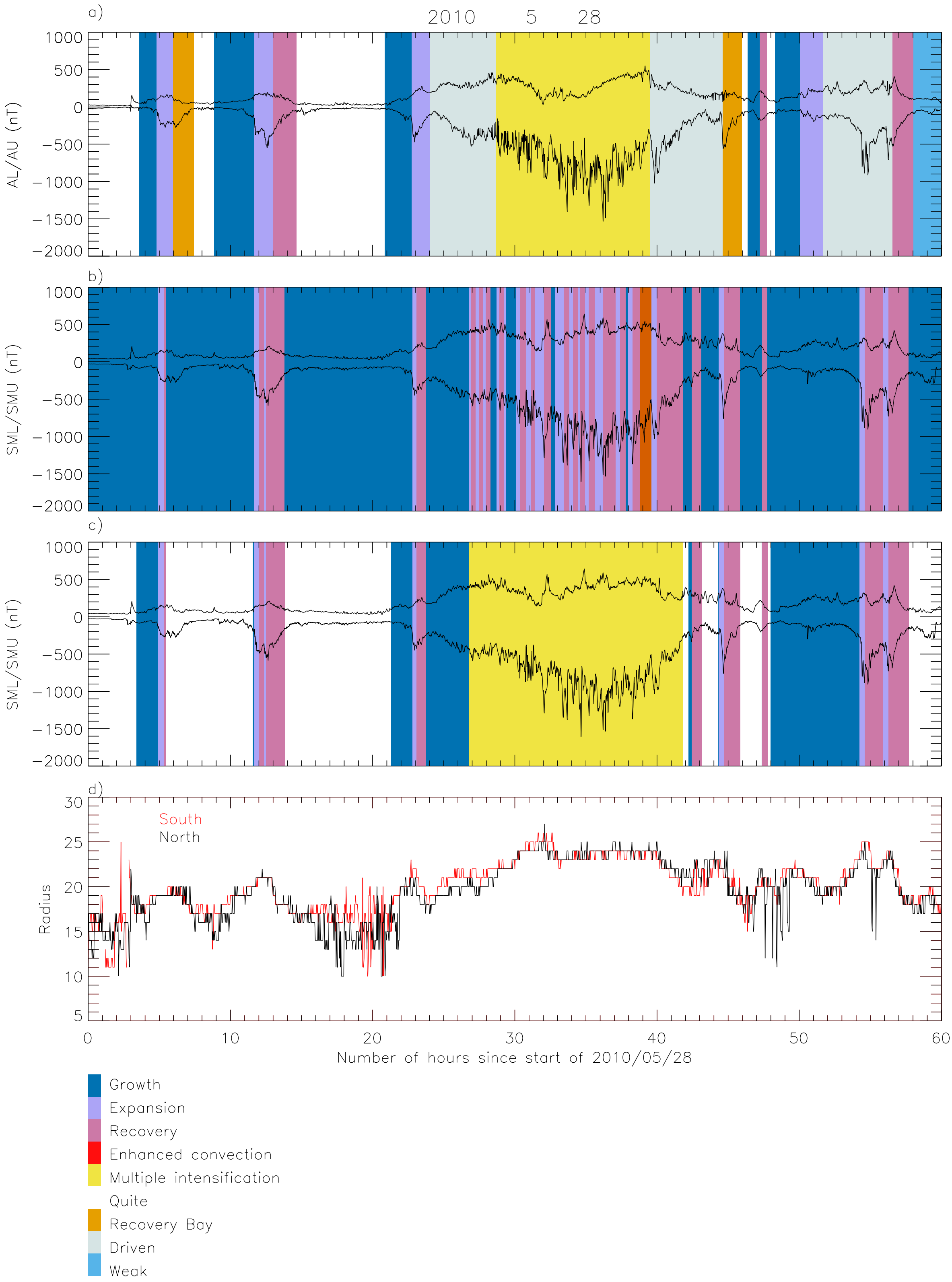
a)
2010 5 28
AL/AU (nT)
b)
SML/SMU (nT)
c)
SML/SMU (nT)
d)
South
North
Radius
Number of hours since start of 2010/05/28
Growth
Expansion
Recovery
Enhanced convection
Multiple intensification
Quite
Recovery Bay
Driven
Weak

Figure 1.

degrees colatitude in the northern hemisphere (black) and southern hemisphere (red) for the same period. If the FAC boundary changes by less than 3° in either hemisphere over five consecutive phases described by SOPHIE, where each phase must be less than 1 hr in length, the five phases are flagged as multiple intensifications. If four consecutive phases are less than 1 hr and at least one of the phases, or the phase before or after is enhanced convection then the phases and the enhanced convection phase are classified as multiple intensification. Less than an hour in length was chosen based on the Milan et al. (2021) definition of multiple intensifications having periods of between 30 and 60 min. The number of consecutive phases was chosen by finding the best fit to multiple events from Milan et al. (2021). We then combine multiple intensification events if there are no growth phases between them. We ensure that a multiple intensification events starts and ends with a growth phase as defined by SOPHIE.

The original SOPHIE classified extended periods of growth phase. These are removed in the SOPHIE-M list and re-classified into growth and quiet phase using the 1 min resolution OMNI data set (King & Papitashvili, 2005). OMNI B_z is used to determine when the interplanetary magnetic field IMF changes from northward to southward closest to the end of a growth phase. Any time before that change is classed as a quiet phase in SOPHIE-M to reduce the number and duration of growth phases, as a growth phase must coincide with southward IMF. Figure 1c shows the SOPHIE-M classification of phases for the same period. The classic substorms are still identified now including a quiet phase before. This does remove some growth phases entirely if there is northward IMF at the end of the phase, such as around 10–11 hr in Figure 1c. The multiple intensification identified by SOPHIE-M is longer than the period identified in the Milan list. It includes some driven phase along with the main rapid variations however does not regularly include classic substorms.

Along with the newly developed SOPHIE-M list we use the SuperMAG SMR indices. As with SymH, SMR does also have some contribution from other current systems but is designed to monitor the ring current. The ring current is not always symmetric particularly during the main phase of a geomagnetic storm but does become more symmetric in the late recovery phase (Newell & Gjerloev, 2012) therefore we use the local time measurements of SMR, (SMR-LT) which are measures of the partial ring current separated by magnetic local time (MLT). They are calculated using all available ground magnetometers from the SuperMAG network at geomagnetic latitudes (MLAT) between −50 and 50°. The baseline removed north component of the magnetic field is used and a correction is applied based on the magnetic latitudes for all stations. Four equally sized local time sectors are used centered at 00, 06, 12 and 18 MLT. The average of each sector's corrected magnetic field data is SMR-LT. SMR is the average of all the SMR-LTs (Gjerloev, 2012; Newell & Gjerloev, 2012). We note that each LT sector will have a different number of observations due to the sparsity of the magnetometer network.

3. Results

We use the Bower, Imber, Milan, Schillings, et al. (2024) list of GMDs and see which SOPHIE-M phase they occur during. Figure 2 shows the frequency of the GMDs for the different phases as classified by the SOPHIE-M list on a magnetic latitude-MLT grid with noon at the top. The number in the top right corner of each panel shows the number of GMDs detected, the percentage of time between 2010 and 2021 that each phase occurs and the percentage of all GMDs that occur in that phase. It is important to note that SOPHIE-M is still over classifying growth time as 50% of the time is classified as growth although this is an improvement on the SOPHIE list. As Milan et al. (2024) showed, the GMDs occur mainly at pre-midnight during the expansion and recovery phase and during the multiple intensification a dawn population is also seen. Few GMDs occur during the quiet (4.5%) and growth phases (5.3%) or during enhanced convection (2.7%). A population of GMDs occurring during quiet times in the 07 to 10 MLT sector has previously been attributed to Kelvin-Helmholtz waves during periods of low geomagnetic activity but fast solar wind (Milan et al., 2023). 59% of GMDs occurred during multiple intensifications, though this phase only accounted for 6% of the total time. The dawnside population during quiet times peaks on the dayside around 7–8 MLT, as opposed to the dawn population of the other phases that peak closer to 5 MLT.

Figure 1. AL and AU indices for 60 hr after the start of 2010/05/28 showing phase classification by: (a) Milan list (b) SOPHIE and (c) SOPHIE-M. Dark blue is the growth phase, lilac is the expansion phase, pink is the recovery phase, red is enhanced convection, yellow is multiple intensification, white is quiet, orange is recovery bay, pale blue is driven and blue is weak. The Milan list uses the OMNI AL and AU indices where the SOPHIE list uses the SuperMAG SMU and SML indices. Panel (d) shows the radius of the boundary between the region 1 and region 2 field aligned current (FACs), calculated by Milan et al. (2015). The northern hemisphere is shown in black and southern hemisphere is shown in red.

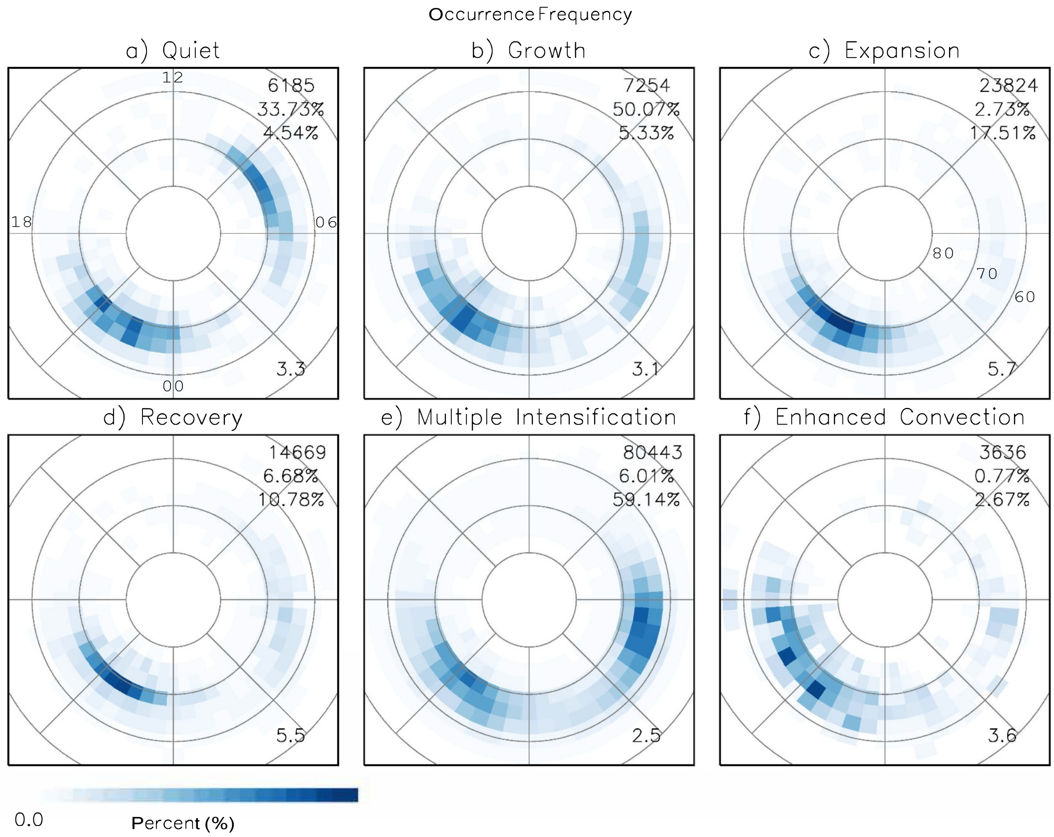

Figure 2. Occurrence frequency of GMDs for different phases as found by SOPHIE-M as a percent of the number of GMD in each phase (a) Quiet (b) Growth (c) Expansion (d) Recovery (e) Multiple intensification and (f) Enhanced convection. The maximum percent of GMDs is given in the lower right hand corner and this is the darkest color on the color scale. The number in the top right shows the number of GMD included in the plot followed by the percentage of time between 2010 and 2021 that each phase occurs and the percentage of the GMD that occur in that phase. Plots are in MLAT and MLT with noon at the top. Concentric circles are 10° latitude.

Figures 3–5 show examples of GMD events. Each figure shows the SML and SMU index in panel (a) with the colors indicating the phase classification from SOPHIE-M as in Figure 1c. Panel (b) shows the Sym-H index with colors indicating the phase of a geomagnetic storm from Walach and Grocott (2019). Panel (c) shows the AsymH index from OMNI. AsymH is a measure of the maximum difference between the 6 low latitude magnetometers used to calculate symH. Panel (d) shows the B_x, B_y, and B_z components of the IMF in GSM coordinate system shown in blue, red, and black, respectively. Panel (e) is the radius of the boundary between the region 1 and region 2 FACs based on Milan et al. (2015). Panel (f) is the MLT, with midnight at the center, of the GMDs color coded by the direction of the magnetic field the GMD is in. Z direction is black, E direction is blue and N direction is red. Panel (g) is the SMR-LT data (Newell & Gjerloev, 2012), SMR06 is green, SMR12 is yellow, SMR18 is red and SMR00 is blue.

The difference between SymH and SMR is that SymH only uses a fixed set of 6 stations where as SMR uses all available ground magnetometers between geomagnetic latitudes of −50 and 50°. The extra benefit of SMR comes from the fact that with more stations the values can be calculated for different local time sectors allowing further investigation of variations on a consistent and global basis (Newell & Gjerloev, 2012).

Event 1 occurred from 14 to 17 July 2012 (Figure 3), during a geomagnetic storm event. Times are quoted as hours since the start of 14 July. The arrival of a solar wind pressure step at around 18 hr lead to a positive excursion in the Sym-H and SMR-LT indices, due to an increase in the magnetopause current. Variable, but mainly northwards, IMF until 30 hr produced low-amplitude fluctuations in Sym-H and SMR-LT. At 30 hr the magnetic cloud arrived with IMF B_z roughly −15 nT, only returning to typical levels around 65 hr. This resulted in a negative excursion in Sym-H and SMR of up to −168 nT, which declined as B_z reduces. The radius of the R1/R2 FACs was

10.1029/2024JA033492

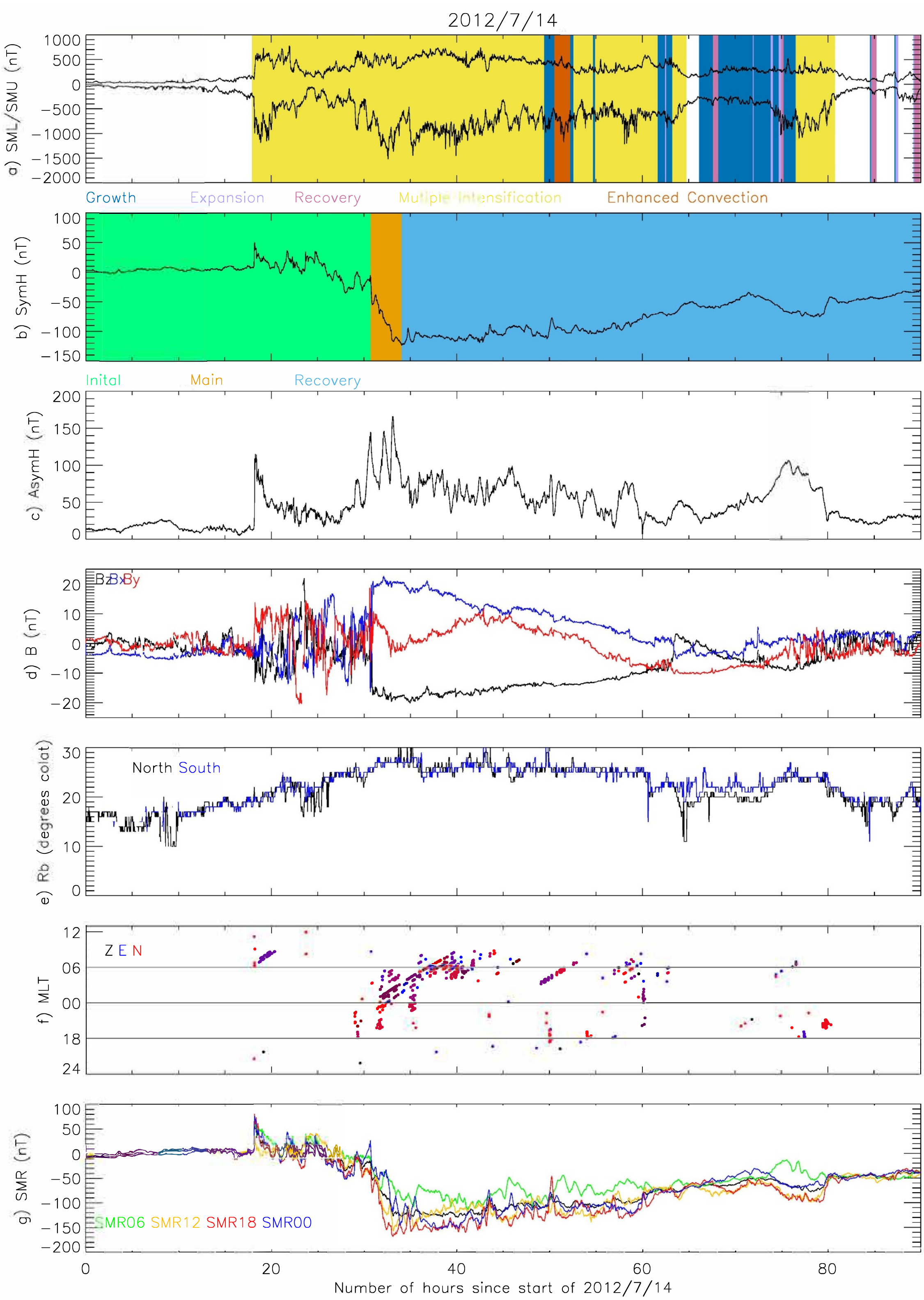

Figure 3. Event 2012/7/14. (a) SML and SMU color-coded with the phases from SOPHIE-M. (b) SymH color-coded based on the Walach and Grocott (2019) storm list. Green is the initial phase, Orange is the main phase and blue is the recovery phase (c) AsymH (d) IMF components z in black, x in blue and y in red (e) colatitude of FAC boundary, northern hemisphere in black and southern hemisphere in blue (f) GMDs location in MLT with midnight at the center and (g) SMR indices SMR06 in green, SMR12 in yellow, SMR18 in red and SMR00 in blue.

Journal of Geophysical Research: Space Physics

10.1029/2024JA033492

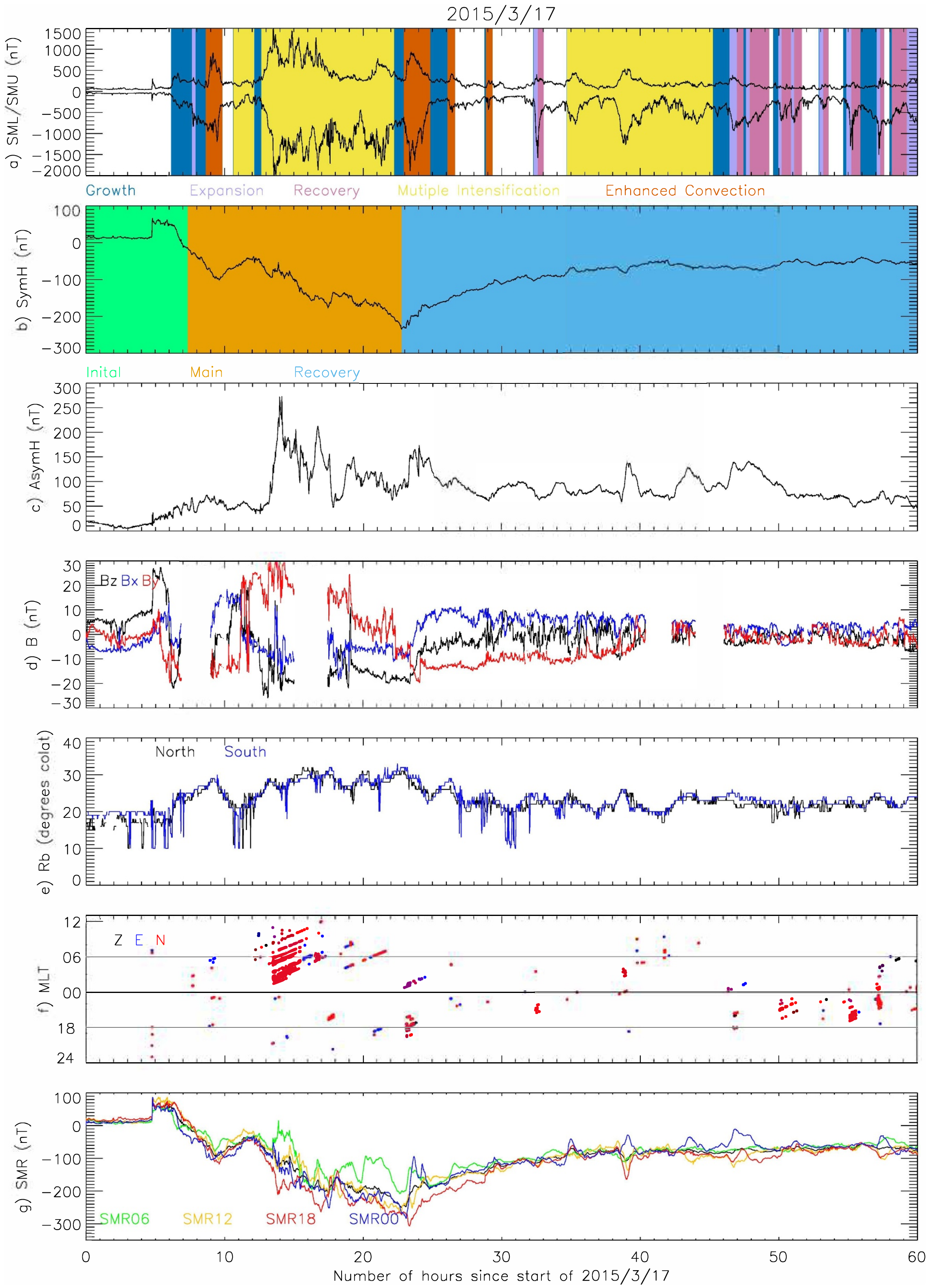

Figure 4. Event 2015/3/17. Same format as Figure 3.

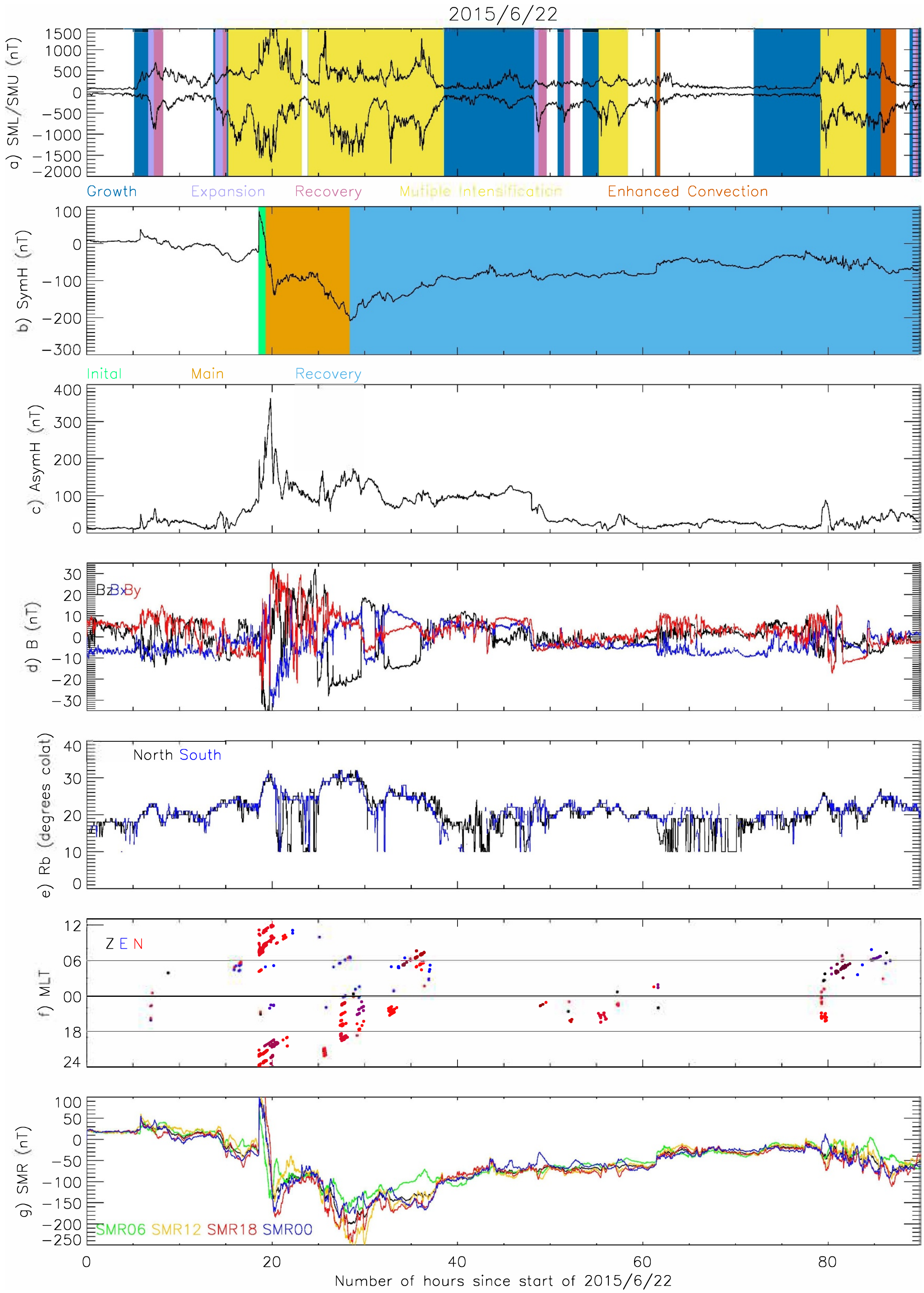

Figure 5. Event 2015/6/22. Same format as Figure 3.

enhanced and uniform throughout the storm. Rapid fluctuations were seen in SML during the storm, such that much of this interval is classified as "multiple intensifications" by SOPHIE-M. At the start of the main phase GMDs were seen in a region straddling 00 MLT as seen in Figure 3f around 30 hr. Subsequently, GMDs were seen in the dawn region, concentrating around 06 MLT between 35 and 60 hr onwards. Another small burst of dawn GMDs was seen between 75 and 78 hr. These dawn GMDs are associated with the variability in SML, that is, this SML activity is produced in the dawn sector and is not associated with substorms (Milan et al., 2024). During the periods when dawn GMDs are observed, the SMR06 index is not as enhanced than the other three local time indices, indicating an asymmetric ring current.

Event 2 occurred from 17 March 2015 to the 20 March 2015 (Figure 4) with time quoted from the start of 17 July. This event is during the well studied St Patrick's' geomagnetic storm. The solar wind pressure step took place around 6 hr causing an increase in Sym-H. The magnetic cloud with mainly southward IMF arrived around 13 hr causing a decrease in Sym-H and SMR to −300 nT, which returned to nominal levels around 35 hr. During this period the maximum difference in then SMR-LT indices was approximately 250 nT as seen by the AsymH index. Through the main phase of the storm the radius of the R1/R2 FACs was enhanced, along with rapid fluctuations seen in SML leading to a SOPHIE-M classification of "multiple intensification" through this period. A second "multiple intensification" interval is identified during the recovery phase starting around 36 hr although the variations in SML are less rapid and have a small magnitude. The main population of GMDs during this event occurred at dawn during the first "multiple intensification" interval during the period of maximum difference between SMR06 and SMR18 indicating an asymmetric ring current. The second "multiple intensification" interval had fewer GMDs associated with it, it can be seen that there is less variability in the SMR-LT values and the IMF components were less intense than during the first period. The end of the time period had many pre-midnight groups of GMDs as would be expected from typical substorm identified by SOPHIE-M.

The final example event is from 22 June 2015 to the 25 June 2015 (Figure 5), with times quoted from the start of 22 June. The event started with a classic substorm around 6 hr that had few GMDs associated with it. There was a positive excursion of Sym-H at around 20 hr likely due to the arrival of a solar wind pressure step. A geomagnetic storm then began with a decrease in the Sym-H and SMR of around 200 nT. This was preceded by northward IMF with a change to southward IMF at around 27 hr. The geomagnetic storm began the late recovery phase around 40 hr with the return of Sym-H to more constant levels of greater than −100 nT. The SOPHIE-M list identified four period of "multiple intensification" where there are rapid fluctuations in the SML index. The radius of the R1/R2 FACs was less uniform through the intervals likely due to the northward IMF periods and the fit from Milan et al. (2015) does not working optimally due to weak FACs. This effect is particularly visible around 62–70 hr. The radius was clearly enhanced through the first and second "multiple intensification" intervals. The main population of GMDs occurred around 20 hr with the largest disturbance in SymH with the GMDs on the dayside. A small dawn group of GMDs preceded this main population and this group coincides with a time when SMR06 was greater than SMR18, indicating an asymmetric ring current. This is also true for the two dawn groups at around 27 and 35 hr. The multiple intensification period found by SOPHIE-M around 55 hr is more likely two substorms rather than multiple intensification, as it does not contain many rapid variations in SML. At the end of the time period shown another multiple intensification phase occurred and dawn GMDs again occurred when the SMR06 was higher than the other SMR indices.

In the example events, the dawn GMDs occur when the SMR06 and SMR18 values have the greatest difference between them. To test this statistically we investigate the difference between the dawn and dusk side low latitude currents (SMR06-SMR18) and the midnight and dayside low latitude currents (SRM00-SMR12) at the time of each GMD from the Bower, Imber, Milan, Schillings, et al. (2024) list between 2010 and 2021. Each panel in Figure 6 shows three intensity maps of SMR00-SMR12 against SMR06-SMR18 with histograms at the top and right of the SMR06-SMR18 values and SMR00-SMR12 values respectively. Figure 6a is for GMDs that occur on the day side between 9 and 17 MLT, Figure 6b is for GMDs that occur at dawn between 2 and 9 MLT and Figure 6c is for GMDs that occur in the pre-midnight sector between 17 and 2 MLT. These MLT ranges are the same as those used by Milan et al. (2023). There are a substantially fewer day GMDs (3401) than dawn (45,208) or pre-midnight (87,402).

The dawn GMDs have a more dispersed intensity map than the pre-midnight or day GMDs. The difference is clear in the SMR06-SMR18 histograms which peaks at around 60 nT for the dawn GMDs and around 0 for the pre-midnight and day GMDs. SMR00-SMR12 histograms all peak at similar values with means of 11.8 nT, 10.9

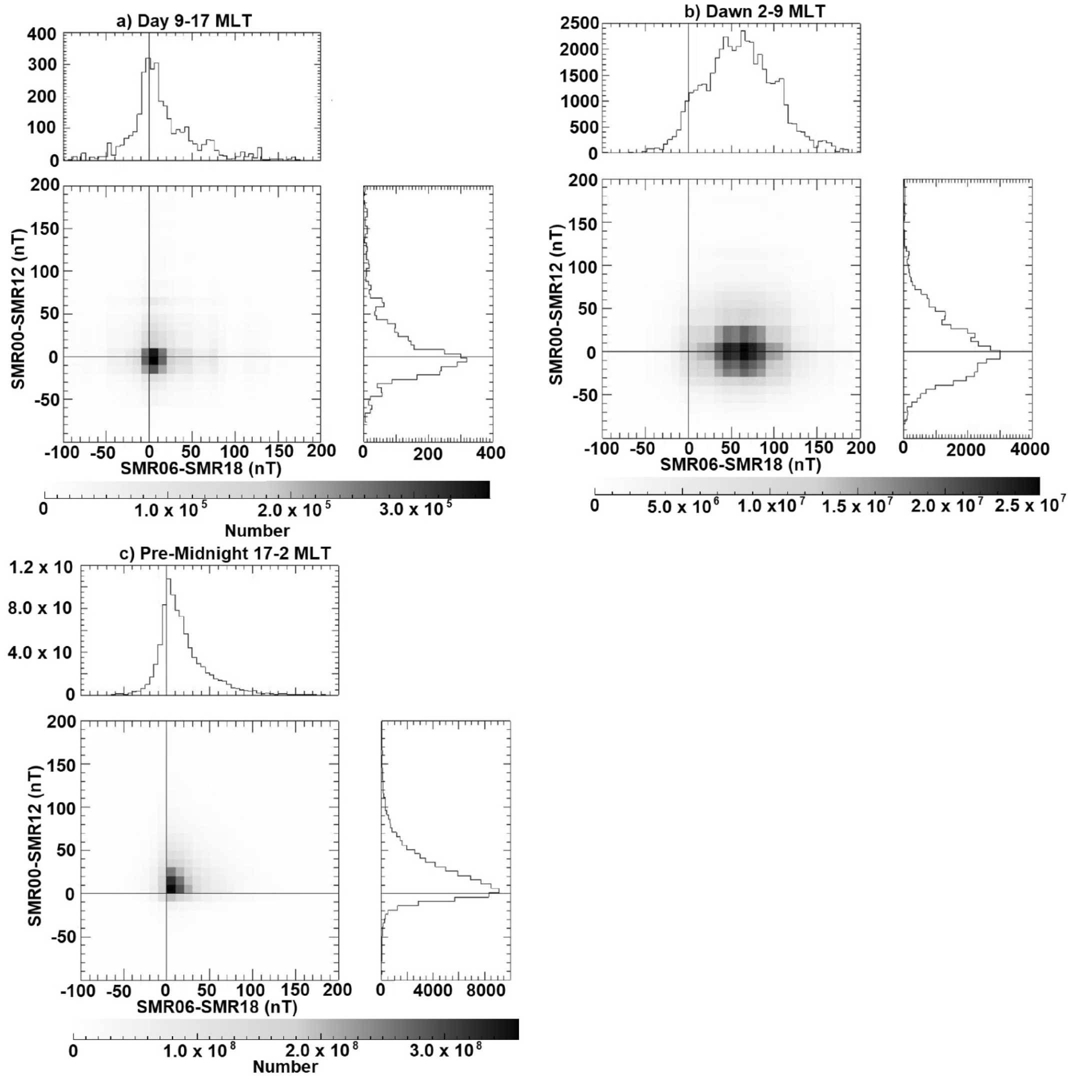

Figure 6. (Main) SMR00-SMR12 against SMR06-SMR18 for each GMD time. Top and right are histograms of the SMR06-SMR18 values and SMR00-SMR12 values respectively. (a) day GMDs (b) dawn GMDs and (c) pre-midnight GMDs.

and 24.3 nT for day, dawn and pre-midnight. The pre-midnight GMD population has the highest mean and is also more skewed than the other data with more GMDs occurring for a positive difference. Pre-midnight GMDs are more likely to occur if SMR00 is greater than SMR12.

4. Discussion

Geomagnetic disturbances during different substorm phases have been investigated using an adapted version of the SOPHIE substorm list (Forsyth et al., 2015) to identify multiple intensification phases, which were described by Milan et al. (2021) as periods of prolonged rapid quasi-periodic variations in AL associated with an expanded auroral oval. The new SOPHIE-M list is not perfect, as seen in Figure 3 some multiple intensification periods can be misclassified as growth and enhanced convection thus increasing the number of GMDs in the growth and enhanced convection phases. Some smaller substorm features are also missed due to the classification criteria of the SOPHIE 90 EPT, resulting in misclassification of related GMDs. There is also ambiguity over the exact start and end time of the multiple intensification phase as it has been taken from the start and end time of phases as described by SOPHIE. The actual start and end time of a multiple intensification may occur during a phase identified by SOPHIE. This issue is most clearly seen when looking at the time during the phases that the GMDs occur.

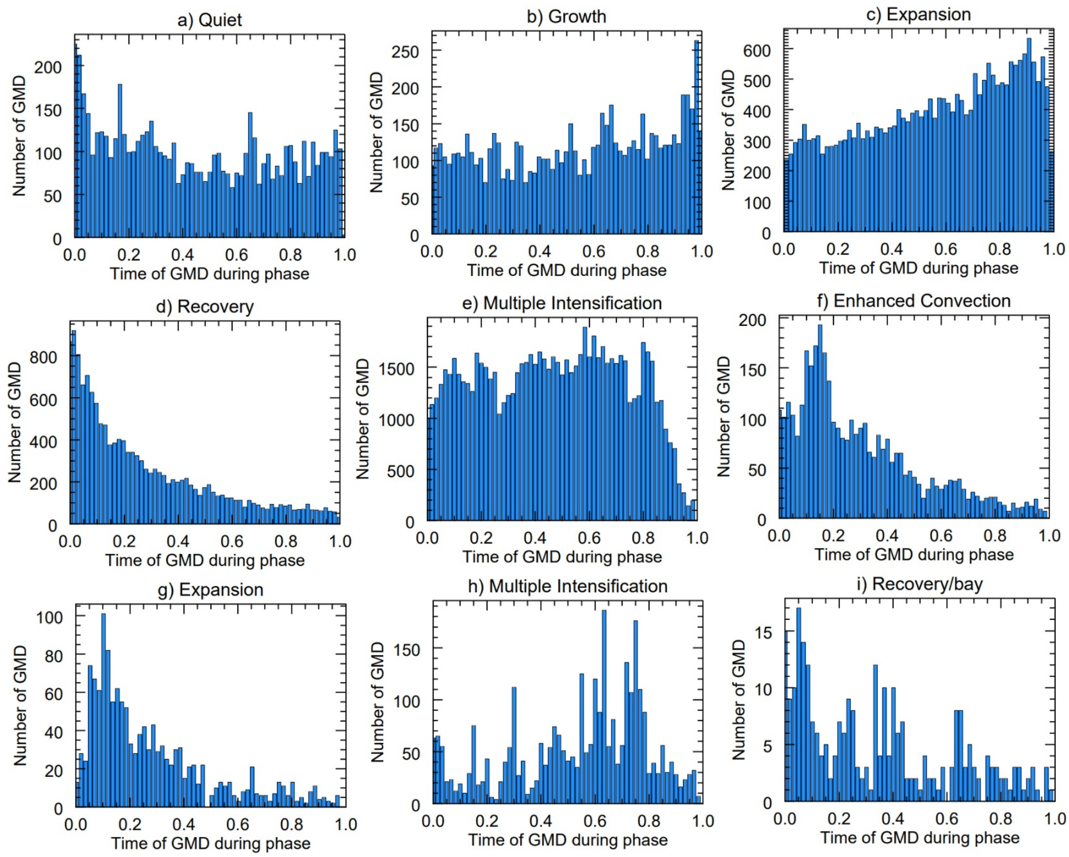

Figure 7. Histograms of the time during the phase that the GMD occur with phases all normalized to their SOPHIE-M list phase (a) Quiet (b) Growth (c) Expansion (d) Recovery (e) Multiple intensification and (f) Enhanced convection. Milan list (g) Expansion (h) Multiple intensification and (i) recovery or recovery bay.

Figure 7 shows histograms of the time during the phase that the GMDs occur when the phases have all been normalized to a duration of an hour in order to see at what point throughout the phase the GMDs occur. From Figures 7a–7f GMDs occur throughout the quiet, growth and multiple intensification phases, toward the beginning of the recovery and enhanced convection and toward the end of the expansion phase. It would be expected that the GMDs should occur toward the beginning of the expansion phase as this is when the largest change in the magnetic field is expected to happen and this is the case for the GMDs that occur during the Milan list defined expansion phase (Figure 7g). The reason GMDs occur toward the end of the SOPHIE-M list expansion phase is because of how the SOPHIE list defines the start of the expansion phase, as discussed above; the start of the phase is incorrectly shifted earlier for large events that will cause the most GMDs. SOPHIE-M is useful however as the Milan list is only available for 2010 and it allows us to investigate other years. It also does well at representing the amount of time that is spent in each convection state.

Milan et al. (2024) showed that the multiple intensification phase occurs for 1.4% of 2010 whereas the SOPHIE-M list has multiple intensifications for 6% of 2010–2021. An increase is expected because 2010 was a quiet year near solar minimum and more multiple intensifications would be expected in more active years. For 2010 SOPHIE-M has multiple intensification phase occurring 3.67% of the time. This is higher than Milan et al. (2024) likely because of the fit from Milan et al. (2015) is not working optimally due to weak FACs and the over-selection of expansion and recovery periods by the SOPHIE list. The expansion phase occurs for a smaller percentage of the time here than in Milan et al. (2024) but the percent of GMDs with in the expansion phase is similar.

Figures 3–5 show three examples of multiple intensification phases as identified by SOPHIE-M. For each event it can be seen that the SMR-LT indices become more variable and less comparable to each other during the multiple intensifications suggesting an asymmetric ring current. The statistical analysis in Figure 6 shows that the dawn

GMDs typically occur when the difference between SMR06 and SMR18 is 50 nT with SMR06 being higher (less negative) than SMR18. This asymmetry of the dawn-dusk ground magnetometers has been shown to be a characteristic feature of the main phase of geomagnetic storms (Ohtani, 2021). Ohtani et al. (2018) suggested the formation of a dawnside current wedge (DCW) based on 4 geomagnetic storm events. They show that there is a significant intensification of the westward electrojet which initially takes place post-midnight and later extends covering the dawn sector. They suggested that the closure of the DCW is by field aligned currents and hence a wedge current is formed. Ohtani (2021) then performed a statistical study on the SuperMAG SMR-LT index during the main phase of 693 geomagnetic storm between 1996 and 2018. They showed that during the main phase of the storms the ratio of SMR06/SMR is usually smaller than SMR18/SMR, where SMR is the average of the 4 SMR local time values. They suggested the formation of two westward auroral electrojets, one at dawn associated with the dawn-dusk asymmetry and one at midnight associated with day-night asymmetry.

This is in agreement with the results found here as the multiple intensification phases typically occur during the main phase of geomagnetic storms as shown by (Milan et al., 2024). We also find that the pre-midnight GMDs, that are thought to be associated with substorms, occur when SMR00 is greater than SMR12 although the relation is not a strong as the SMR06/SMR18 for the dawn GMDs, which is in agreement with the formation of the substorm current wedge. Ohtani et al. (2021) investigated isolated substorms and showed that the mid-latitude magnetic field increases on the nightside and decreases on the dayside, correlated with the nightside westward auroral electrojet intensity. Ohtani (2021) therefore suggests that it is the substorm wedge current system that is the primary cause of the day-night asymmetry of ground magnetic depression.

Our results are also in agreement with the modeling results of Sorathia et al. (2023). They showed that a dawn-dusk asymmetry of low latitude ground perturbations could be caused by mesoscale bursty bulk flows in the dawnside inner magnetosphere. Milan et al. (2024) showed that dawn GMDs are produced by eastwards-drifting auroral omega bands and streamers, which could be the auroral manifestation of these BBFs. Sorathia et al. (2023) go on to suggest that the DCW could explain the preference for dawn geomagnetically induced currents. We have shown here that a DCW is a related to dawn GMDs with the large difference between the SMR06 and SMR18 values at the time of dawn GMDs.

5. Conclusion

The SOPHIE 90 EPT substorm list has been adapted to identify periods of multiple intensifications which are prolonged rapid quasi-periodic variations in the AL index associated with an expanded auroral oval. The multiple intensification convection state occurs 6% of the time between 2010 and 2021 but contains 59% of geomagnetic disturbances (GMDs) with magnitudes of over 50 nT in 10 s as found by Bower, Imber, Milan, Schillings, et al. (2024). Pre-midnight GMDs occur primarily in the substorm expansion and recovery phases and occur during intervals of day-night asymmetry in the low latitude current and are likely associated with the substorm current wedge. Recent models suggest the formation of a "dawnside current wedge" (DCW) during the main phase of storms that could lead to GMDs. We have shown that dawn GMDs occur most frequently during the multiple intensification state and are associated with a large dawn-dusk asymmetry in the low latitude current likely associated with a DCW.

Data Availability Statement

The 1-s cadence ("high fidelity") SuperMAG data were obtained through the SuperMAG portal at https://supermag.jhuapl.edu/mag/?fidelity=high (Gjerloev, 2012). The high resolution (1-min) OMNI data used in this study were obtained from the NASA Goddard Space Flight Center (GSFC) Space Physics Data Facility OMNIWeb portal at https://omniweb.gsfc.nasa.gov/form/om_filt_min.html (King & Papitashvili, 2005). The AMPERE current map data used by (Milan et al., 2015) to determine the field-aligned current boundary used in this study can be obtained from https://ampere.jhuapl.edu/download/ (Anderson et al., 2002). The FAC radius data can be accessed via https://doi.org/10.25392/leicester.data.11294861.v1 (Milan, 2019). The SOPHIE list 2010–2022 90 EPT is available at https://doi.org/10.5522/04/27014701.v1 (Forsyth, 2024). The Bower, Imber, Milan, Schillings, et al. (2024) GMD list is available at https://doi.org/10.25392/leicester.data.26954074.v1 (Bower, Imber, & Milan, 2024). The SOPHIE-M list created using the algorithm described and used in this paper is available at https://doi.org/10.25392/leicester.data.28143227.v1 (Bower et al., 2025).

Acknowledgments

GEB, SMI and SEM were supported by the Natural Environment Research Council (NERC), UK, Grant NE/W006766/1. We acknowledge use of NASA/GSFC's Space Physics Data Facility's CDAWeb service (at http://cdaweb.gsfc.nasa.gov) and OMNI data. AS was supported by Vetenskaprådet, Swedish Research Council, Grant VR 2021-06683. ALF is supported by an STFC studentship. For the purpose of open access, the author has applied a Creative Commons Attribution (CC BY) license to the Author Accepted Manuscript version arising from this submission. This research used the ALICE High Performance Computing facility at the University of Leicester. For the ground magnetometer data we gratefully acknowledge: INTERMAGNET, Alan Thomson; CARISMA, PI Ian Mann; CANMOS, Geomagnetism Unit of the Geological Survey of Canada; The S-RAMP Database, PI K. Yumoto and Dr. K. Shiokawa; The SPIDR database; AARI, PI Oleg Troshichev; The MACCS program, PI M. Engebretson; GIMA; MEASURE, UCLA IGPP and Florida Institute of Technology; SAMBA, PI Eftyhia Zesta; 210 Chain, PI K. Yumoto; SAMNET, PI Farideh Honary; IMAGE, PI Liisa Juusola; Finnish Meteorological Institute, PI Liisa Juusola; Sodankylä Geophysical Observatory, PI Tero Raita; UiT the Arctic University of Norway, Tromsø Geophysical Observatory, PI Magnar G. Johnsen; GFZ German Research Centre For Geosciences, PI Jürgen Matzka; Institute of Geophysics, Polish Academy of Sciences, PI Anne Neska and Jan Reda; Polar Geophysical Institute, PI Alexander Yahnin and Yarolav Sakharov; Geological Survey of Sweden, PI Gerhard Schwarz; Swedish Institute of Space Physics, PI Masatoshi Yamauchi; AUTUMN, PI Martin Connors; DTU Space, Thom Edwards and PI Anna Willer; South Pole and McMurdo Magnetometer, PI's Louis J. Lanzarotti and Alan T. Weatherwax; ICESTAR; RAPIDMAG; British Artarctic Survey; McMac, PI Dr. Peter Chi; BGS, PI Dr. Susan Macmillan; Pushkov Institute of Terrestrial Magnetism, Ionosphere and Radio Wave Propagation (IZMIRAN); MFGI, PI B. Heilig; Institute of Geophysics, Polish Academy of Sciences, PI Anne Neska and Jan Reda; University of L'Aquila, PI M. Vellante; BCMT, V. Lesur and A. Chambodut; Data obtained in cooperation with Geoscience Australia, PI Andrew Lewis; AALPIP, co-PIs Bob Clauer and Michael Hartinger; MagStar, PI Jennifer Gannon; LISN PI Cesar Valladares; SuperMAG, PI Jesper W. Gjerloev; Data obtained in cooperation with the Australian Bureau of Meteorology, PI Richard Marshall. References to the AMPERE technique can be found in Milan et al. (2015). We gratefully acknowledge the use of AMPERE data provided by JHU/APL, PIs Brian Anderson/Sarah Vines.

References

Albertson, V., Thorson, J. M., Clayton, R. E., & Tripathy, S. C. (1973). Solar-induced-currents in power systems: Cause and effects. *IEEE Transactions on Power Apparatus and Systems*(2), 471–477. https://doi.org/10.1109/TPAS.1973.293746

Anderson, B. J., Takahashi, K., Kamei, T., Waters, C. L., & Toth, B. A. (2002). Birkeland current system key parameters derived from Iridium observations: Method and initial validationn results. *Journal of Geophysical Research*, *107*(A6), SMP11-1–SMP11-13. https://doi.org/10.1029/2001JA000080

Apatenkov, S., Pilipenko, V., Gordeev, E., Viljanen, A., Juusola, L., Belakhovsky, V., et al. (2020). Auroral omega bands are a significant cause of large geomagnetically induced currents. *Geophysical Research Letters*, *47*(6), e2019GL086677. https://doi.org/10.1029/2019GL086677

Bower, G. E., Imber, S. M., & Milan, S. E. (2024a). Gmd list 2010-2022 [Dataset]. *University of Leicester*. https://doi.org/10.25392/leicester.data.26954074.v1

Bower, G. E., Imber, S. M., & Milan, S. E. (2025). Sophie-m list [Dataset]. *University of Leicester*. https://doi.org/10.25392/leicester.data.28143227.v1

Bower, G. E., Imber, S. M., Milan, S. E., Schillings, A., Fleetham, A. L., & Gjerloev, J. W. (2024b). Location of geomagnetic disturbances in relation to the field aligned current boundary. *Journal of Geophysical Research: Space Physics*, *129*(10), e2024JA033039. https://doi.org/10.1029/2024JA033039

Campbell, W. H. (1978). Induction of auroral zone electric currents within the Alaska pipeline. *Pure and Applied Geophysics*, *116*(6), 1143–1173. https://doi.org/10.1007/BF00874677

Clilverd, M. A., Rodger, C. J., Freeman, M. P., Brundell, J. B., Mac Manus, D. H., Dalzell, M., et al. (2021). Geomagnetically induced currents during the 07–08 september 2017 disturbed period: A global perspective. *Journal of Space Weather and Space Climate*, *11*, 33. https://doi.org/10.1051/swsc/2021014

Coxon, J. C., Chisham, G., Freeman, M. P., Forsyth, C., Walach, M.-T., Murphy, K. R., et al. (2023). Extreme birkeland currents are more likely during geomagnetic storms on the dayside of the earth. *Journal of Geophysical Research: Space Physics*, *128*(12), e2023JA031946. https://doi.org/10.1029/2023JA031946

Fleetham, A. L., Milan, S. E., Imber, S. M., Bower, G. E., Gjerloev, J. W., & Vines, S. K. (2024). The relationship between large dB/dt and field-aligned currents during five geomagnetic storms. *Journal of Geophysical Research: Space Physics*, *129*(7), e2024JA032483. https://doi.org/10.1029/2024JA032483

Forsyth, C. (2024). Sophie list 2010-2022, ept 90. UCL [Dataset]. https://doi.org/10.5522/04/27014701.v1

Forsyth, C., Rae, I. J., Coxon, J. C., Freeman, M. P., Jackman, C. M., Gjerloev, J. W., & Fazakerley, A. N. (2015). A new technique for determining substorm onsets and phases from indices of the electrojet (sophie). *Journal of Geophysical Research: Space Physics*, *120*(12), 10–592. https://doi.org/10.1002/2015JA021343

Freeman, M. P., Forsyth, C., & Rae, I. J. (2019). The influence of substorms on extreme rates of change of the surface horizontal magnetic field in the United Kingdom. *Space Weather*, *17*(6), 827–844. https://doi.org/10.1029/2018SW002148

Gjerloev, J. W. (2012). The SuperMAG data processing technique. *Journal of Geophysical Research*, *117*(A9), A09213. https://doi.org/10.1029/2012JA017683

Juusola, L., Viljanen, A., Van De Kamp, M., Tanskanen, E., Vanhamäki, H., Partamies, N., & Kauristie, K. (2015). High-latitude ionospheric equivalent currents during strong space storms: Regional perspective. *Space Weather*, *13*(1), 49–60. https://doi.org/10.1002/2014SW001139

King, J. H., & Papitashvili, N. E. (2005). Solar wind spatial scales in and comparisons of hourly wind and ace plasma and magnetic field data. *Journal of Geophysical Research*, *110*(A2), A02104. https://doi.org/10.1029/2004JA010649

Marshall, R. A., Waters, C. L., & Sciffer, M. D. (2010). Spectral analysis of pipe-to-soil potentials with variations of the Earth's magnetic field in the Australian region. *Space Weather*, *8*(5), S05002. https://doi.org/10.1029/2009SW000553

Milan, S. E. (2019). Ampere r1/r2 fac radii [Dataset]. *University of Leicester*. https://doi.org/10.25392/leicester.data.11294861.v1

Milan, S. E., Bower, G. E., Fleetham, A. L., Imber, S. M., Schillings, A., Gjerloev, J. W., et al. (2024). Characteristics and causes of large dB/dt events in the pre-midnight and dawn sectors. *Journal of Geophysical Research: Space Physics*, *129*(10), e2024JA032811. https://doi.org/10.1029/2024JA032811

Milan, S. E., Carter, J. A., Korth, H., & Anderson, B. J. (2015). Principal component analysis of birkeland currents determined by the active magnetosphere and planetary electrodynamics response experiment. *Journal of Geophysical Research: Space Physics*, *120*(12), 10–415. https://doi.org/10.1002/2015JA021680

Milan, S. E., Carter, J. A., Sangha, H., Bower, G. E., & Anderson, B. J. (2021). Magnetospheric flux throughput in the dungey cycle: Identification of convection state during 2010. *Journal of Geophysical Research: Space Physics*, *126*(2), e2020JA028437. https://doi.org/10.1029/2020JA028437

Milan, S. E., Imber, S. M., Fleetham, A. L., & Gjerloev, J. W. (2023). Solar cycle and solar wind dependence of the occurrence of large db/dt events at high latitudes. *Journal of Geophysical Research: Space Physics*, *128*(4), e2022JA030953. https://doi.org/10.1029/2022JA030953

Newell, P. T., & Gjerloev, J. W. (2012). Supermag-based partial ring current indices. *Journal of Geophysical Research*, *117*(A5), A05215. https://doi.org/10.1029/2012JA017586

Ngwira, C. M., Sibeck, D., Silveira, M. V., Georgiou, M., Weygand, J. M., Nishimura, Y., & Hampton, D. (2018). A study of intense local d b/dt variations during two geomagnetic storms. *Space Weather*, *16*(6), 676–693. https://doi.org/10.1029/2018SW001911

Ohtani, S. (2021). Revisiting the partial ring current model: Longitudinal asymmetry of ground magnetic depression during geomagnetic storms. *Journal of Geophysical Research: Space Physics*, *126*(9), e2021JA029643. https://doi.org/10.1029/2021JA029643

Ohtani, S., Gjerloev, J. W., Anderson, B. J., Kataoka, R., Troshichev, O., & Watari, S. (2018). Dawnside wedge current system formed during intense geomagnetic storms. *Journal of Geophysical Research: Space Physics*, *123*(11), 9093–9109. https://doi.org/10.1029/2018JA025678

Ohtani, S., Imajo, S., Nakamizo, A., & Gjerloev, J. W. (2021). Globally correlated ground magnetic disturbances during substorms. *Journal of Geophysical Research: Space Physics*, *126*(4), e2020JA028599. https://doi.org/10.1029/2020JA028599

Ohtani, S., Sorathia, K., Merkin, V., Frey, H., & Gjerloev, J. W. (2023). External and internal causes of the stormtime intensification of the dawnside westward auroral electrojet. *Journal of Geophysical Research: Space Physics*, *128*(10), e2023JA031457. https://doi.org/10.1029/2023JA031457

Partamies, N., Weygand, J. M., & Juusola, L. (2017). Statistical study of auroral omega bands. *Annales Geophysicae*, *35*(5), 1069–1083. https://doi.org/10.5194/angeo-35-1069-2017

Patterson, C. J., Wild, J. A., Beggan, C. D., Richardson, G. S., & Boteler, D. H. (2024). Modelling electrified railway signalling misoperations during extreme space weather events in the UK. *Scientific Reports*, *14*(1), 1583. https://doi.org/10.1038/s41598-024-51390-3

Pulkkinen, A., Pirjola, R., & Viljanen, A. (2008). Statistics of extreme geomagnetically induced current events. *Space Weather*, *6*(7), S07001. https://doi.org/10.1029/2008SW000388

Rogers, N. C., Wild, J. A., Eastoe, E., & Huebert, J. (2021). Climatological statistics of extreme geomagnetic fluctuations with periods from 1 s to 60 min. *Space Weather*, *19*(11), e2021SW002824. https://doi.org/10.1029/2021SW002824

Schillings, A., Palin, L., Opgenoorth, H. J., Hamrin, M., Rosenqvist, L., Gjerloev, J. W., et al. (2022). Distribution and occurrence frequency of db/dt spikes during magnetic storms 1980–2020. *Space Weather*, *20*(5), e2021SW002953. https://doi.org/10.1029/2021SW002953

Sorathia, K., Michael, A., Merkin, V., Ohtani, S., Keesee, A., Sciola, A., et al. (2023). Multiscale magnetosphere-ionosphere coupling during stormtime: A case study of the dawnside current wedge. *Journal of Geophysical Research: Space Physics*, *128*(11), e2023JA031594. https://doi.org/10.1029/2023ja031594

Viljanen, A. (1997). The relation between geomagnetic variations and their time derivatives and implications for estimation of induction risks. *Geophysical Research Letters*, *24*(6), 631–634. https://doi.org/10.1029/97GL00538

Walach, M.-T., & Grocott, A. (2019). Superdarn observations during geomagnetic storms, geomagnetically active times, and enhanced solar wind driving. *Journal of Geophysical Research: Space Physics*, *124*(7), 5828–5847. https://doi.org/10.1029/2019JA026816

Weigel, R. S., Vassiliadis, D., & Klimas, A. J. (2002). Coupling of the solar wind to temporal fluctuations in ground magnetic fields. *Geophysical Research Letters*, *29*(19), 1915. https://doi.org/10.1029/2002GL014740

Zou, Y., Dowell, C., Ferdousi, B., Lyons, L. R., & Liu, J. (2022). Auroral drivers of large db/dt during geomagnetic storms. *Space Weather*, *20*(11), e2022SW003121. https://doi.org/10.1029/2022SW003121